

Comparison of PBM and ANPM Models for Predicting Grinding Product Size Distributions

Juan Camilo Luján González^a, Juan Pablo Restrepo Lopera^a

Santiago Builes Toro^b

^a Process Engineering Student, EAFIT University, Medellín Colombia

^b Professor, Project Advisor, Department of Process Engineering, EAFIT University, Medellín, Colombia

Abstract

Grinding is a very important industrial operation that draws up to 4% of the global electricity consumption. It is imperative to predict accurately the appropriate retention times necessary for a given size reduction to minimize the wasted energy invested in overgrinding. However, the most common models for scaling, such as Bond, could lead to a design risk on the order of $\pm 20\%$ due to their assumption that a single particle size can describe the entire particle size distribution. Thus, different approaches (both phenomenological and non-phenomenological) need to be explored.

In the present work, a population balance model is compared with an algebraic statistical model, to predict the evolution of particle size distribution over time, assessing them in terms of accuracy, robustness, and computational complexity. Even though the population balance model had a lower accuracy and higher mathematical complexity its predictions were physically coherent, which made it a more robust model for extrapolating to different initial conditions and milling times. It is important to note that due to the 2020 COVID-19 pandemic, experimental information was limited, which inhibited an independent validation of the models, and an overfitting analysis for the ANPM.

1. Introduction

Grinding of solid particles is an important process found in a large number of industries, such as cement, mining, chemicals and foods [1]. Comminution draws up to 4% of the global electrical energy [2] which could be in part explained by its low efficiency, as it is estimated that only 1% of the total energy input to the grinding system is directly responsible of the size reduction of the particles [1].

Reducing the size of solid materials is an operation difficult to describe quantitatively due to the inherent complexity of grinding processes [3], for this reason it is usual to find simplified expressions (e.g. laws of Kick, Rittinger and Bond) that only relate one size range parameter of the material being crushed for calculating the energy needed to increase the surface area of the material [4], [5]. However, these expressions ignore the different subprocesses (i.e. breakage kinetics, transport of material through the mill, size classification) that make up a grinding circuit, and could lead to a design risk on the order of $\pm 20\%$, meaning that the specific power would require an oversizing of 20% for trustworthy results, affecting both the capital and the operation cost for the process equipment [6].

Therefore, more complex grinding size-energy models are required to provide accurate and cost-saving results. For instance, learning the kinetic behavior of the grinding process would provide appropriate retention times in which the particle size will be satisfactorily reduced, which not only minimizes energy consumption but also avoids overgrinding valuable solids [7].

For these purposes different alternatives have been proposed, one of the most important is to treat size reduction phenomena as processes analogous to irreversible chemical reactions. In this approach, larger particles

(reactants) can break into smaller ones (products) [8], formulating kinetic models based on population balances, that is, on mass balances for each particle size, depending on grinding time [8], [9].

Several studies have been carried out to evaluate the predictive capacity of population balance models (PBM), Kotake et al. [10] studied the effects on the grinding rate constant with respect to variations in the particle size distribution (PSD) of the feed and the diameter of the mill balls. The authors developed mathematical expressions that explain their experimental behavior. Similarly, Gupta [11] also verified the significant effect of the PSD on the specific breakage rate of the particles, finding that the latter varies with the type of material, displaying a greater effect in the case of softer materials and thicker particles. In a subsequent work, Gupta presented a detailed study of the variations in the production rate of a ball mill with generation of fine particles [12], which provides relevant information for improving the scaling of production systems.

A number of different robust models have been developed in order to predict the product size of a ball mill in batch operation, for example, Tavares et al. [13] formulated a model that considers the distribution of stressing energies in the mill and the distribution of fracture energies of particles contained, which allowed to explore the orders of breakage in more detail. Capece et al. [14] went beyond the phenomenology considered by classical PBM and derived a breakage model that takes into account interparticle interactions, using discrete element method simulations of a grinding ball impacting a confined particle bed; further investigation in this model could improve control and design of grinding processes.

An algebraic, non-phenomenological model (ANPM) is generally used when models based on principles are either unavailable or too difficult to implement. In the case of grinding of solid particles, where time profiles are required, the model must consider time variations. An example of this is the design of dynamic experiments, a recently developed methodology that is based on the classical approach of design of experiments and allows considering time-variant batch systems [15]–[17], however, due to the lack of dynamic variables in this specific process, the design of dynamic experiments cannot be applied to a simple grinding process.

The present work is focused on assessing the accuracy, robustness, and complexity of both PBM and an ANPM for predicting the PSD of clay brick processed in a batch ball mill as function of the initial PSD and grinding time. This might aid also in the understanding of the material breakage mechanism as well as its kinetic behavior. In order to achieve the aforementioned, this research aims to perform a comparison of the predictive capabilities of an ANPM and a PBM in terms of the mean absolute error (MAE) and maximum absolute error (MAX), while robustness comparison was performed with three hypothetic simulated scenarios. Finally, computational complexity was evaluated qualitatively analyzing the equations that make up each model and the methods involved in their resolution.

2. Materials and methods

In order to study the predictive capability of PBMs against an ANPM, a clay brick was initially ground until all particles could fit through a $1\frac{1}{2}$ in mesh (all used sieves were in the scale according to ASME E11 [18]). Afterwards, the material was characterized with a sieve set of meshes No. 5, No .10, A clay brick was initially ground and sieved using a set of meshes $1\frac{1}{2}$ in, No. 5, No. 10 and the collector pan. The material retained in the two middle sieves was utilized for the grinding experiments. Two experiments¹ of grinding and sieving were performed, which consisted in the evaluation of the PSD at different geometric succession milling times [6] (1.0, 2.0, 4.0, 8.0, 16.0 and 32.0 minutes). For each run, the rotational speed was constant at 109 rpm, while fractional ball filling and fractional material filling (calculated with the packed density) was 2.3% and 2.9%, respectively.

The mill was filled with alumina balls with the following properties:

¹ It was not possible to perform any additional experiments due to the shutdown of the research facilities during the 2020 COVID-19 sanitary emergency.

Table 1. Properties of grinding media

Number of balls	30
Average mass [g/ball]	34.51
Average packed density [g/cm ³]	8.96
Average volume [cm ³ /ball]	3.85
Average diameter [cm]	2.97
Standard deviation of the diameter [cm]	0.24

A ceramic batch ball mill with 19 cm of diameter and length of 17.5 cm and sieve numbers of No. 5, No. 10, No. 35, and No. 60 was used for achieving the previous purpose. In order to have three differentiated groups of particle sizes, the mass remaining on sieve No. 5 will be referred to as **M1**, the retained in sieves No. 10, No. 35 and No. 60 will be grouped and called **M2**, and what is left in the collector will be labeled as **M3**.

Parametrization of each model was performed based on the experimental data. Below is a brief description of each model and its adjustment algorithm:

- PBM consists on mass balances for each size range i at time t , which is expressed mathematically as [19]:

$$\frac{dm_i(t)}{dt} = -k_i * [m_i(t)]^\alpha + \sum_{j=1}^{i-1} b_{ij} * k_j * [m_j(t)]^\beta \quad (1)$$

In (1) m_i is the mass fraction of i , k_i is the function of the breakage rate of i , b_{ij} is the breakage distribution function which is defined as the proportion of size range i that is transformed into size range j , finally α and β correspond to the reaction orders, in the same way as in a chemical system.

For each size range i there is a differential equation like (1), so each grinding and sieving run has an algebraic-differential system that was solved numerically with the data set of all the runs, based on the Runge-Kutta-Fehlberg numerical method and minimizing the MAX between the predicted and the experimental value. This was performed using the solver tool in Microsoft Excel.

- ANPM: The authors developed an ANPM, based on the classic design of experiments, which is described by the equation below:

$$x_{i,t} = b_o + b_i * x_{i,0} + b_t * t + b_{ii} * x_{i,0}^2 + b_{tt} * t^2 + b_{it} * x_{i,0} * t \quad (2)$$

Where b_o , b_i , b_{ii} , b_{tt} and b_{it} are the regression coefficients that are obtained by the method of ordinary least squares, where $x_{i,t}$ is the mass fraction of size range i , in a grinding time t and $x_{i,0}$ is the initial mass fraction of the size fraction i . Both $x_{i,0}$ and t are in coded form, that is, between -1 and +1.

Equation 2 was applied to **M1** and **M3**, while the values of **M2** were calculated with mass balances.

After adjusting the models to the experimental data, they were compared based on their accuracy, robustness, and computational complexity. Accuracy was represented by MAE and MAX, robustness was analyzed with three hypothetic simulated scenarios, while computational complexity was evaluated qualitatively analyzing the equations that make up each model and the methods required for solving them.

3. Results and analysis

3.1. Experimental data

The two grinding experiments were performed according to the description above. Figure 1 contains the profiles depicting the evolution of PSD over time.

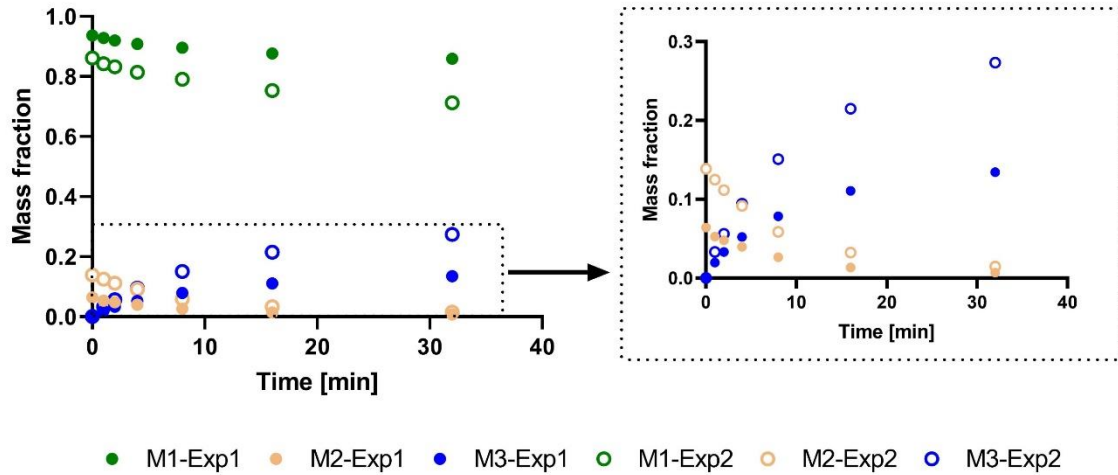


Figure 1. Experimental mass fractions retained in M1, M2, M3, opened symbols are used for experiment 1 (Exp1) and closed are for experiment 2 (Exp2). Inset corresponds to a zoomed in view of the dashed region of the left figure.

Most of the initial feed material corresponded to the coarsest particle size (**M1**), and the constant decrease that it presents in both runs can be explained by two factors; first, because bigger particles have a higher chance to collide and generate smaller particles, and second, since there is no coarser material, no new **M1** material is generated. Also, **M2** did not show material accumulation, which could suggest that abrasion is the most dominant breakage mechanism, where big particles produce several small particles and another big particle. According to Little et al. [20] abrasion is generally triggered by two phenomena: localized low intensity surface stresses or repeated low energy contacts, both could be happening inside the mill. The previously statement seems to agree with experimental observations, during the experimental runs edges in particles of **M1** were worn out after each milling, which could explain the rapid generation of **M3**, especially in the early phases of the process.

3.2. Fitted models and accuracy

3.2.1. PBM

The equation 3, 4 and 5 embody the PBM for the three differentiated size ranges, where Ma , Mb and Mc are the mass fractions of M1, M2 and M3, respectively.

$$\frac{dMa}{dt} = -k_1 Ma^\delta \quad (3)$$

$$\frac{dMb}{dt} = -k_2 Mb^\omega + k_1 b_{21} Ma^\delta \quad (4)$$

$$\frac{dMc}{dt} = k_1 b_{31} Ma^\delta + k_2 b_{32} Mb^\omega \quad (5)$$

After the fitting process, the authors obtained several solutions that minimized the MAX, so it was selected the one with the lowest Akaike information criterion (51.33). The MAE that corresponds to this model is 0.013 and the MAX is 0.049, both in terms of mass fraction. The parameters' values are shown in Table 2

Table 2. Constants of the selected PBM

k_1 [1/min]	0.005
k_2 [1/min]	0.200
b_{21}	2/3
b_{31}	1/3
b_{32}	1.0
δ	1.0
ω	1.0
$k_1 b_{21}$ [1/min]	0.003
$k_1 b_{31}$ [1/min]	0.002
$k_2 b_{32}$ [1/min]	0.200

It is noteworthy that the kinetic orders previously shown are both equal to 1. This means that the breakage follows an exponential kinetic relation. Also, from the previous results it is possible to estimate that 67% of the clay of size **M1** breaks into **M2**, while 33% of the former turns into **M3** sized material.

One of the advantages of PBM as a phenomenological model is that it lets conclude certain behaviors in the process. Evidence of this is shown in Table 2, where the $k_i b_{ij}$ constants represent the rates in which the material breaks from one specific size (j) range to another (i). This concept is simplified in Figure 2. From these values it is possible to analyze how the rate in which **M1** transforms into **M2** (0.003/min) is higher than the rate in which **M1** turn into **M3** (0.002/min). At the same time, the rate in which **M1** turns into **M3** is lower than the one **M2** turns into **M3** (0.200/min).

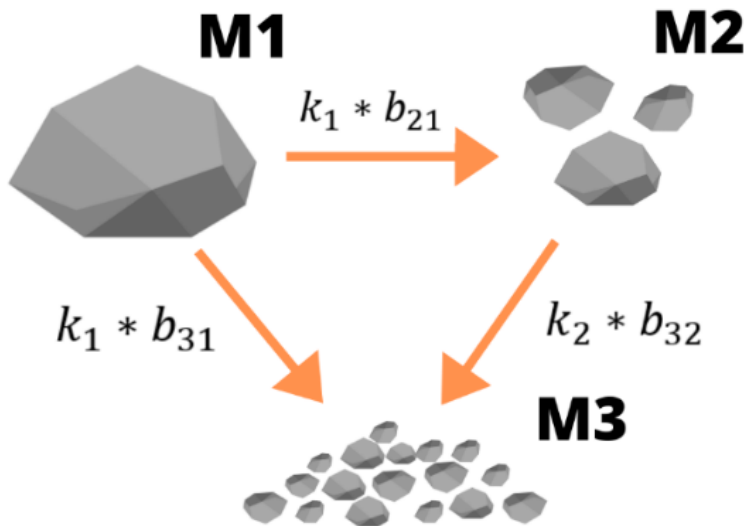


Figure 2. Depiction of the rates in which the material breaks from one specific size range to another

Figure 3 illustrates the comparison of the values of mass fractions observed in the experiments and the ones predicted by the fitted model.

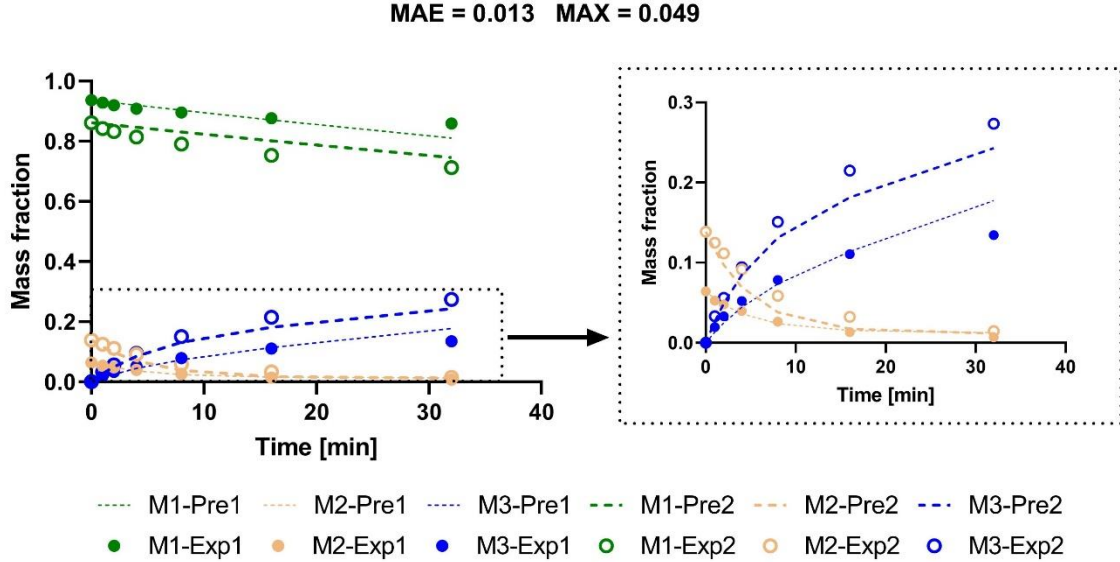


Figure 3. Mass fractions retained experimentally and predicted with PBM for M1, M2 and M3. Opened symbols are used for experiment 1 (Exp1) and closed are for experiment 2 (Exp2). Thick dashed lines correspond to the prediction of experiment 1 (Pre 1), while thin dashed lines correspond to the prediction of experiment 2 (Pre 2). Inset shows a zoomed in view of the dashed region of the left figure.

In order to have a deeper understanding of the model, its residuals were analyzed in terms of homoscedasticity and expected value. PBM's residuals did not follow a normal distribution, this was inferred with Shapiro-Wilk test ($p - value = 0.02252$), so the expected value could not be calculated using a typical confidence interval for the mean. Based on the previously stated, the authors implemented a non-parametric method based on the Bootstrap sampling [21] in order to estimate with a 95% confidence an interval for the median, which resulted in (-0.0018 to 0.0061). It must be noted that as zero is contained in the interval, it is not possible to reject that the residuals' expected value is not zero

The second criterion was the homoscedasticity of the residuals. Since the PBM is not a linear regression and its residuals do not follow a normal distribution, $F - test$ nor Breusch-Pagan can be utilized. Therefore, the vastly robust and non-parametric, Fligner-Killeen [22], [23] test was applied, allowing to conclude that there are significant differences ($p - value = 0.02575$) between the variance residuals of the first and second experiments; in other words the model is heteroscedastic. Still, it is important to keep in mind that homoscedasticity is not a requirement for PBM, as it is not a linear regression based model.

3.2.2. ANPM

After verifying statistical significance of each term, the models that resulted are the depicted below:

$$x_{M1,t} = 0.424 + 0.571 * x_{M1,0} - 0.026 * t + 0.009 * t^2 + 0.032 * x_{M1,0} * t \quad (6)$$

$$x_{M3,t} = 0.694 + 0.696 * x_{M3,0} - 0.019 * t \quad (7)$$

$$x_{M2,t} = 1 - x_{M3,t} - x_{M1,t} \quad (8)$$

The model's MAE is 0.004 and the MAX is 0.016, both in terms of mass fraction, from which it is possible to observe that both measures are lower in the ANPM than in the PBM.

Figure 4 shows the graphic comparison between the experimental results and the predictions for each of the size ranges. It could be noted that this model fits better than PBM, which can be asserted as, it not only follows the curve more smoothly, but also it reaches the last experimental point in all cases.

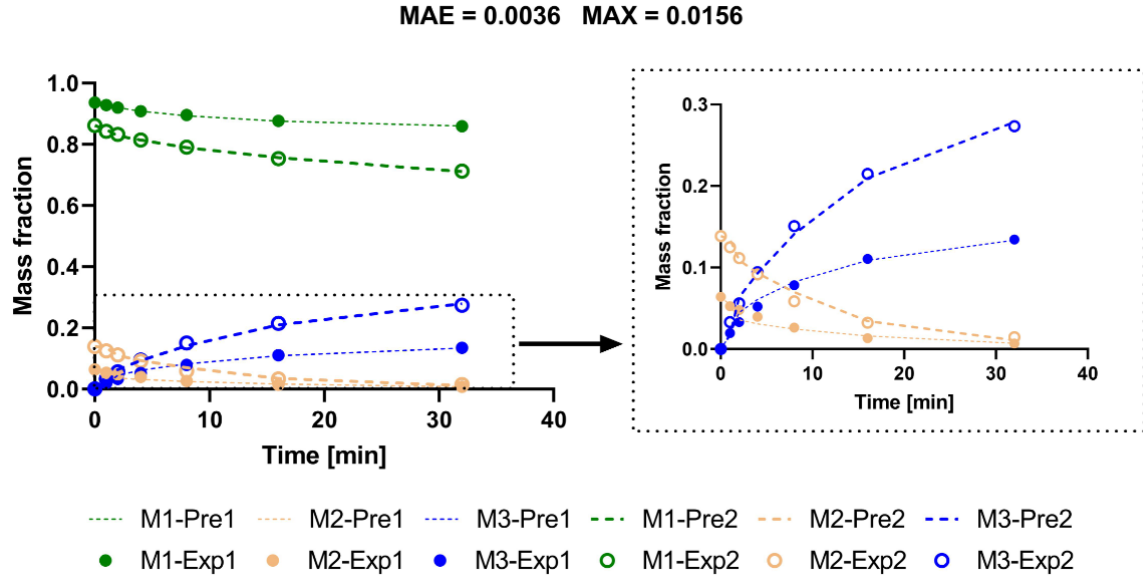


Figure 4. Mass fractions retained experimentally and predicted with ANPM for M1, M2 and M3. Opened symbols are used for experiment 1 (Exp1) and closed are for experiment 2 (Exp2). Thick dashed lines correspond to the prediction of experiment 1 (Pre 1), while thin dashed lines correspond to the prediction of experiment 2 (Pre 2). Inset shows a zoomed in view of the dashed region of the left figure.

Residuals analysis was also performed for ANPM, and it was possible to conclude that for both the equation 6 and 7, the residuals followed a normal distribution, since the Shapiro-Wilk test's null hypothesis was not rejected for any of the cases (*p - values* were 0.538 and 0.902, respectively). Due to the previous, the expected value of the residuals could be estimated with 95% confidence an interval for the mean, resulting in (-0.005 to 0.005). Analogous to PBM, zero is contained in the mean interval, so it is not possible to reject that the residuals' expected value is not zero. Homoscedasticity was not discarded by the Breusch-Pagan test, with *p - values* of 0.582 for equation 6, and 0.223 for equation 7. The previous is a good result as homoscedasticity is a requirement for linear models adjusted with ordinary least squares.

3.3. Robustness analysis

In order to perform the robustness comparison, three hypothetic scenarios were simulated with the two models. The initial PSDs are presented in Table 3. They are different from the experimental conditions and the milling time was extrapolated up to 128 minutes, which is four times longer than the final experimental time. Figure 5 depicts the PSD evolution plots for these three hypothetic scenarios for both models.

Table 3. Initial PSD for the three scenarios

Scenario	Initial PSD		
	M1	M2	M3
1	85%	4%	12%
2	65%	31%	4%
3	62%	4%	35%

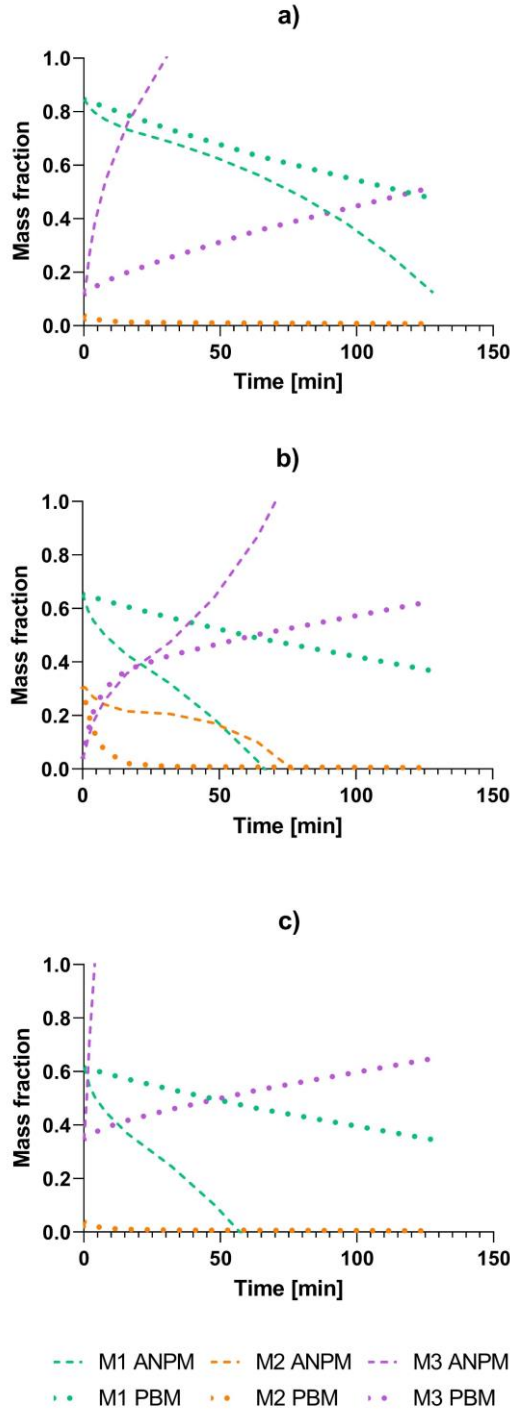


Figure 5. PSD evolutions for the three cases and both models, where a) is Scenario 1, b) is Scenario 2 and c) corresponds to Scenario 3. PBM and ANPM are represented by dotted and dashed lines, respectively.

It can be noted that while PBM respects mass conservation principle, ANPM fails to maintain physical coherence, as it predicts mass fractions below zero and over one, this is shown in Figure 6, which displays the complete ANPM simulation results. Although the statistical model was more accurate for fitting the

experimental data than the phenomenological one, it is not a reliable model for predicting new conditions outside the initial experimental range.

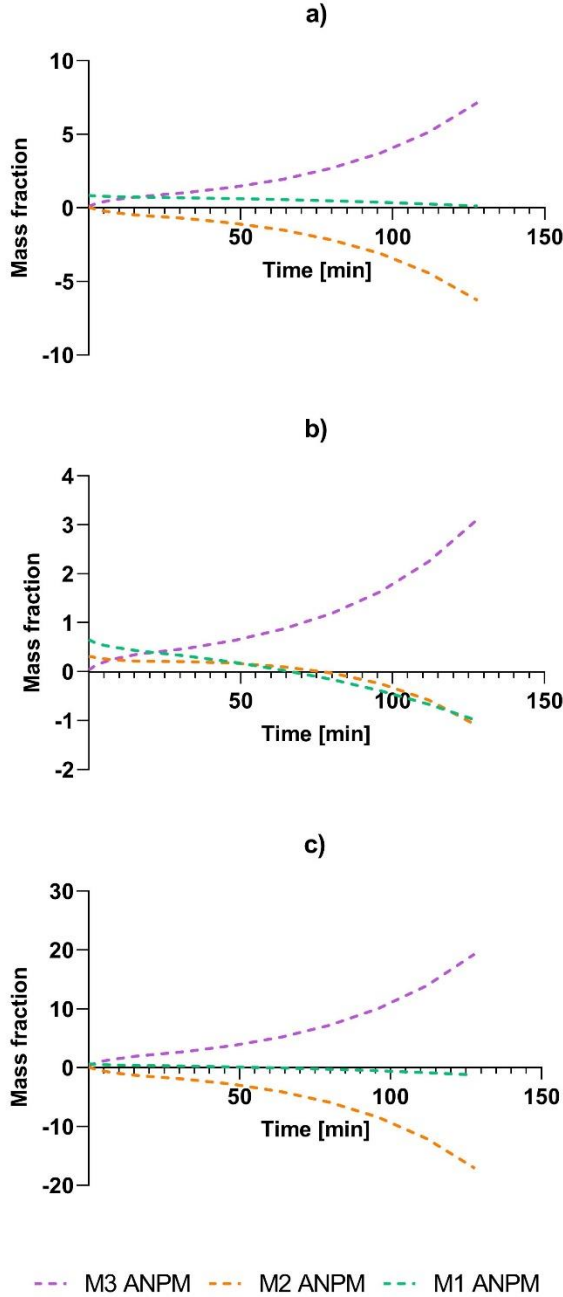


Figure 6. Complete PSD evolutions for the three cases simulated with ANPM, where a) is Scenario 1, b) is Scenario 2 and c) corresponds to Scenario 3.

ANPM tends to predict quicker increases in M3 and quicker decreases of M1, in comparison to PBM. Also, the higher the initial M3 mass fraction is, the faster the ANPM will predict incoherent mass fractions. On the other hand, PBM is a phenomenological model, and for that reason its predictions respect the physical principles, which make it a more robust model for extrapolating to different initial conditions and milling times.

3.4. Computational complexity

To analyze the computational complexity of each model it is important to notice that to adjust the PBM of this study, a system of three differential equations with seven parameters had to be solved, and in order to perform this, a numerical method had to be employed, tandem a minimization of the maximum error. In contrast ANPM only needs to adjust two algebraic equations with 12 parameters, applying ordinary least squares method, which is quite simpler.

It is important to state that during the search of a better model, the parameters of ANPM to be fitted was reduced to eight, while PBM's parameters were reduced to two, which means that PBM has more degrees of freedom than ANPM.

4. Conclusions

From the accuracy analysis it was concluded that ANPM fitted better to the experimental data, with a MAE of 0.004 and a MAX of 0.016, as opposed to PBM, from which resulted a slightly higher MAE and MAX of 0.013 and 0.049, respectively. This can be expected due to the fact of PBM having more degrees of freedom than ANPM. Nevertheless, this apparent higher accuracy did not guaranteed consistency when the models were used to predict from extrapolated initial conditions and milling times, where PBM, as a phenomenological model outputted physically coherent results, while ANPM predicted mass fractions below zero and over one. This reinforces the need of validation through independent scenarios when comparing phenomenological and non-phenomenological models.

The previously stated allows to conclude that although the statistical model was more accurate for fitting the experimental data than the phenomenological one, it is not a reliable model for predicting new conditions outside the initial experimental range.

Another important conclusion is that the experimental data suggested that abrasion was the main breakage mechanism. On the other hand, due to the phenomenological nature of PBM it was possible to calculate the rates in which the material breaks for each of the size ranges, wherein the rate in which **M1** transformed into **M2** (0.003/min) is higher than the rate in which the former turned into **M3** (0.002/min). At the same time, the rate in which **M2** turned into **M3** (0.200/min) is higher than the one where **M1** transformed into **M3**.

References

- [1] W. L. McCabe, J. C. Smith, y P. Harriott, *Unit Operations of Chemical Engineering*, 7th ed. New York, NY: McGraw-Hill, 2004.
- [2] D. W. Fuerstenau, *Comminution and Energy Consumption*. Washington, D.C.: National Academies Press, 1981.
- [3] M. Maleki-Moghaddam, M. Yahyaei, y S. Banisi, «A method to predict shape and trajectory of charge in industrial mills», *Miner. Eng.*, vol. 46-47, pp. 157-166, jun. 2013.
- [4] D. W. Green y R. H. Perry, *Perry's Chemical Engineers' Handbook*, 8.^a ed. New York, NY, 2008.
- [5] V. K. Gupta, «An appraisal of the energy-size reduction relationships for mill scale-up design», *Adv. Powder Technol.*, vol. 30, n.^o 1, pp. 73-84, 2019.
- [6] J. . Herbst y D. . Fuerstenau, «Scale-up procedure for continuous grinding mill design using population balance models», *Int. J. Miner. Process.*, vol. 7, n.^o 1, pp. 1-31, may 1980.
- [7] T. Eisele y S. Kawatra, «Design of iron ore comminution circuits to minimize overgrinding», *2006 SME Annu. Conf. - Adv. Comminution*, pp. 309-320, 2006.
- [8] T. J. Napier-Munn, S. Morrell, R. D. Morrison, y T. Kojovic, *Mineral Comminution Circuits Their Operation and Optimisation*, 1.^a ed. Brisbane: Julius Kruttschnitt Mineral Research Centre, 1996.
- [9] H. Dundar, H. Benzer, y N. Aydogan, «Application of population balance model to HPGR crushing», *Miner. Eng.*, vol. 50-51, pp. 114-120, sep. 2013.
- [10] N. Kotake, K. Suzuki, S. Asahi, y Y. Kanda, «Experimental study on the grinding rate constant of solid materials in a ball mill», *Powder Technol.*, vol. 122, n.^o 2-3, pp. 101-108, ene. 2002.
- [11] V. K. Gupta, «Effect of size distribution of the particulate material on the specific breakage rate of particles in dry ball milling», *Powder Technol.*, vol. 305, pp. 714-722, ene. 2017.

- [12] V. K. Gupta, «Understanding production of fines in batch ball milling for mill scale-up design using the population balance model», *Adv. Powder Technol.*, vol. 29, n.^o 9, pp. 2035-2047, sep. 2018.
- [13] L. M. Tavares y R. M. de Carvalho, «Modeling breakage rates of coarse particles in ball mills», *Miner. Eng.*, vol. 22, n.^o 7-8, pp. 650-659, jun. 2009.
- [14] M. Capece, R. N. Davé, y E. Bilgili, «On the origin of non-linear breakage kinetics in dry milling», *Powder Technol.*, vol. 272, pp. 189-203, mar. 2015.
- [15] C. Georgakis, «Design of Dynamic Experiments: A Data-Driven Methodology for the Optimization of Time-Varying Processes», *Ind. Eng. Chem. Res.*, vol. 52, n.^o 35, pp. 12369-12382, sep. 2013.
- [16] E. C. Martínez, M. D. Cristaldi, y R. J. Grau, «Design of Dynamic Experiments in Modeling for Optimization of Batch Processes», *Ind. Eng. Chem. Res.*, vol. 48, n.^o 7, pp. 3453-3465, abr. 2009.
- [17] A. Fiordalis y C. Georgakis, «Data-driven, using design of dynamic experiments, versus model-driven optimization of batch crystallization processes», *J. Process Control*, vol. 23, n.^o 2, pp. 179-188, feb. 2013.
- [18] ASTM, «Standard Specification for Woven Wire Test Sieve Cloth and Test Sieves ASTM E-11 17». ASME, 2017.
- [19] R. Zhao, Y. Han, M. He, y Y. Li, «Grinding kinetics of quartz and chlorite in wet ball milling», *Powder Technol.*, vol. 305, pp. 418-425, ene. 2017.
- [20] L. Little, A. N. Mainza, M. Becker, y J. Wiese, «Fine grinding: How mill type affects particle shape characteristics and mineral liberation», *Miner. Eng.*, vol. 111, n.^o May 2016, pp. 148-157, sep. 2017.
- [21] B. Efron, «Bootstrap Methods: Another Look at the Jackknife», *Ann. Stat.*, vol. 7, n.^o 1, pp. 1-26, abr. 1979.
- [22] W. J. Conover, M. E. Johnson, y M. M. Johnson, «A Comparative Study of Tests for Homogeneity of Variances, with Applications to the Outer Continental Shelf Bidding Data», *Technometrics*, vol. 23, n.^o 4, pp. 351-361, nov. 1981.
- [23] M. A. Fligner y T. J. Killeen, «Distribution-Free Two-Sample Tests for Scale», *J. Am. Stat. Assoc.*, vol. 71, n.^o 353, pp. 210-213, mar. 1976.